Grand canonical Monte Carlo Simulations of the hydration interaction between oligo(ethylene glycol)-terminated alkanethiol self-assembled monolayers

ARTICLE *in* THE JOURNAL OF PHYSICAL CHEMISTRY B · NOVEMBER 2002

Impact Factor: 3.3 · DOI: 10.1021/jp0257471

3 AUTHORS, INCLUDING:

Tomohiro Hayashi
Tokyo Institute of Technology
74 PUBLICATIONS **1,130** CITATIONS

SEE PROFILE

Grand Canonical Monte Carlo Simulations of the Hydration Interaction between Oligo(ethylene glycol)-Terminated Alkanethiol Self-Assembled Monolayers

Alexander J. Pertsin, Tomohiro Hayashi, and Michael Grunze*

Angewandte Physikalische Chemie, Universität Heidelberg, INF 253, D-69120 Heidelberg, Germany

Received: March 11, 2002; In Final Form: July 22, 2002

The hydration forces operating between two parallel methoxy tri(ethylene glycol)-terminated alkanethiol self-assembled monolayers (SAMs) immersed in water are simulated using the grand canonical Monte Carlo technique, the TIP4P model for water, and a quantum chemistry-based force field for the SAM−water interactions. Two structural modifications of the SAMs are studied, one assembled on the Ag(111) and the other on the Au(111) substrate. Both the Ag- and Au-supported SAMs show typical hydrophobic behavior: the water-mediated interaction between the SAMs is attractive, and the water density level between the SAMs is noticeably reduced. In addition, at small separations, the SAMs induce capillary evaporation of the confined water. The Ag- and Au-supported SAMs show substantial differences in their interfacial behavior, which can be attributed to the difference in the areal density between the SAMs. The simulation results are discussed in the context of the experimentally observed differences in protein adsorption properties and surface force behavior between the Ag- and Au-supported SAMs.

1. Introduction

The forces operating between surfaces, colloid particles, and molecules in water play an important part in colloid chemistry, biology, and other areas. In particular, they are responsible for colloidal stability, micelle formation, biomembrane fusion, and the resistance of surfaces to protein adsorption.[1−4] While on the subject of surfaces, it is common practice to classify the interactions between two surfaces immersed in water into four types: (i) direct interactions between the surfaces, (ii) interactions arising from the surface-induced redistribution of ions present in water, (iii) interactions caused by the adsorption of nondissociating impurities on the surfaces, and (iv) so-called "hydration" interactions, which are associated with surface-induced changes in the structure of water itself. (A similar classification applies to colloid particles and molecules). The first two types of interaction are explained by the classical DLVO theory[3] in terms of direct van der Waals attraction between the surfaces and electrostatic double-layer repulsion between the ions. In later studies,[5] the treatment of the electrostatic energy was improved by including a correlation (fluctuation) contribution to the electrostatic energy. The interactions caused by nondissociating impurities can be described on the basis of a general thermodynamic analysis of the forces experienced by two adsorbing plates in gases and multicomponent liquids.[6]

The most challenging task in interpreting water-mediated interactions is to describe hydration forces. The existing theories[7−9]are based on assumed microscopic mechanisms and approximations whose adequacy is difficult to verify experimentally because of the lack of the relevant structural knowledge. In such a situation, one has to resort to the methods of computer simulation. Unfortunately, direct simulations of hydration forces are very few in number because of considerable computational difficulties involved in the simulation of open confined water systems (Figure 1). In all of these few simulations, the water−surface interaction is modeled with simple laterally homogeneous potentials, which neglect completely the atomistic structure of the confining surfaces as well as the effect of water on this structure.

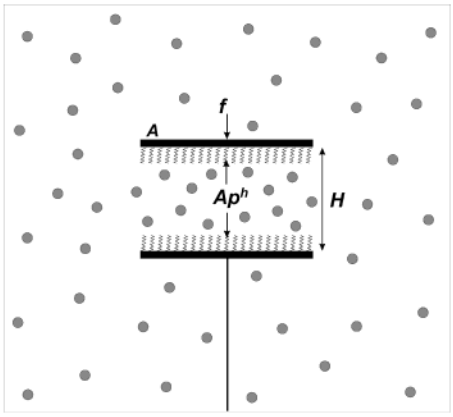

Figure 1. System of two parallel plates of area A that are covered with SAMs and immersed in water; the plates repel each other with force Ap^h. p^h is the hydration pressure, and f is the external force applied in surface-force experiments to keep the surfaces at a given separation H.

In this paper, we extend the simulations of hydration forces to real surfaces, as formed by self-assembled monolayers (SAMs) of long-chain organic molecules. In the past decade, these monolayer systems have received both experimental[10,11] and theoretical[12] interest as ideal model surfaces for studying molecular adsorption, adhesion, wetting, lubrication, and other surface and interfacial phenomena. In addition, SAMs are promising systems for practical use in chemical sensing, thin-film nonlinear optics, biocompatibility, and lithography.[10,13] The calculations described in this paper are concerned with methoxy tri(ethylene glycol) (hereafter, EG3-OMe) -terminated alkanethiols, $HS(CH_2)_n(OCH_2CH_2)_3OCH_3$, self-assembled on the (111) surfaces of gold and silver. For the sake of computational simplicity, the alkane chain is taken to be short, $n = 3$.

* Corresponding author. E-mail: michael.grunze@urz.uni-heidelberg.de.

10.1021/jp025747l CCC: $22.00
Published on Web 10/25/2002

Comparative simulations with $n = 3$ and 10 did not reveal a perceptible effect of the alkane chain length on the interaction of the SAMs with water.

A remarkable feature of the EG3-OMe-terminated SAMs is a strong dependence of their properties on the substrate used. Thus, the Au-supported SAMs repel each other in aqueous electrolyte solutions, whereas the SAMs on Ag show attraction.[14] Also, the SAMs prepared on Au are resistant to protein adsorption, whereas those on Ag are not.[15] An attempt to explain the difference in protein resistance between the Au- and Ag-supported SAMs was undertaken by Wang et al.[16] on the basis of the experimental finding[15] that the EG3-OMe tails in the Au-supported SAMs assume a nearly helical conformation, whereas those on Ag represent planar all-trans zigzags. Ab initio SCF calculations[16] of the interaction of water with idealized crystal-like SAM models showed that the perfect SAM built up of helical EG3-OMe conformers easily accommodated water molecules on its topmost oxygen atoms to form strong hydrogen bonds of the O···H−O type. By contrast, the structure of the SAM built up of planar conformers did not provide water molecules access to the top oxygen atoms, with the result that the SAM−water interaction was much weaker. Later on, sum frequency generation (SFG) experiments by Zolk et al.[17] showed, however, that the contact with water led to conformational disordering of the Au-supported SAM, which made the idealized SAM model[16] inadequate.

The computer simulation study described below will provide a detailed molecular-level description of the structure of the SAM−water interfacial region as well as quantitative estimates of the water-mediated forces operating between the SAMs. This knowledge will allow us to check whether the experimentally observed differences between the properties of the Au- and Ag-supported SAMs can be explained in terms of structural differences and hydration interactions. Some preliminary results of our simulations have been reported elsewhere.[18,19]

2. Computational Details

In our simulations, the interactions of water molecules with themselves were described with the four-site TIP4P model.[20] The summation of water−water interactions was performed using a spherical cutoff (SC) scheme with a cutoff radius of 7.5 Å. Test simulations with a cutoff radius of 8.5 Å gave very similar results: the deviations for the hydration pressure were within the statistical uncertainty of the calculation. The preference of the SC summation scheme over the minimal image and cylindrical cutoff images in simulations of confined water was demonstrated by Shelley and Patey.[21] The SC scheme was shown to provide nearly the same results as the Ewald method while being computationally much cheaper.

The interactions of water with the SAMs, as well as the interactions within the SAMs, were described using an extension of the quantum chemistry-based atomistic force field developed by Smith et al.[22] for the shortest oligo(ethylene glycols) (OEG) and their complexes with water. The transferability of this force field to EG3-OMe and its complexes with water was tested in our recent work[23] against ab initio electronic structure calculations based on density functional theory (DFT).[24] The Smith et al.[22] force field was extended to cover the alkane chains and their junction with the EG3-OMe tails using the relevant potential functions from the atomistic potential set suggested by Sorensen et al.[25] for alkyl ethers. The interaction of a water molecule with an EG3-OMe-terminated alkanethiol chain in the SAM was cut off if the distance between the water oxygen atom and the nearest atom of the chain exceeded 15 Å. To describe the interaction of the monolayers with the metal substrate, the force field was complemented with the nonbonded and surface corrugation potentials from our early study of alkanethiol−Au SAMs[26] (force field I).

The simulated system represented a thick layer of water confined between two parallel SAMs and allowed the exchange of molecules with a fictitious bulk water reservoir (Figure 1). The chemical equilibrium between the confined and bulk water was maintained using the grand canonical Monte Carlo (GCMC) technique. In generating the Markov chain of configurations of the system, four types of moves were attempted: (i) a displacement of a water molecule, (ii) an insertion of a water molecule, (iii) a deletion of a water molecule, and (iv) a move of a chain in the SAM. No attempt to delete or create a chain comprising the SAM was undertaken, so the areal density of the chains remained constant.

A water molecule, considered to be a rigid body, was displaced by translating its center of mass by a random vector and then rotating it by a random angle about one of the three space-fixed axes chosen at random.[27] To improve the efficiency of insertions and deletions, the excluded-volume mapping method[28] and a Swendsen−Wang filter[29] based on the evaluation of the van der Waals energy of the system were employed. The chain molecules in the SAM were treated as flexible but subject to bond-length constraints.[30] In addition, the position of the two hydrogen atoms attached to a carbon atom, C′, was constrained by maintaining the H−H vector perpendicular to the C−C′−X plane and the midpoint of this vector on the bisector of the C−C′−X angle (X = S, C, or O). The bond-length constraints were implemented using the rotational displacement procedure based on the rotation of a chain backbone atom around the virtual bond linking its two neighboring backbone atoms.[30] One move of a randomly selected chain was defined to include a positional displacement of the chain as a whole and successive rotational displacements of all of its backbone atoms, starting with the sulfur headgroup and ending with the terminal carbon atom.

The simulation box represented a rectangular prism with dimensions L_x, L_y, and L_z. The substrate of the lower SAM was placed at $z = 0$ parallel to the $x-y$ plane. In the x and y dimensions, the system was replicated periodically. The lateral dimensions L_x and L_y were taken to be multiples of the SAM lattice periods a and b to conform to the periodic boundary conditions. The particular dimensions used were $L_x = 6a$ and $L_y = 3b = 3\sqrt{3}a$, where $a = 5.01$ and 4.6 Å for the gold and silver substrates, respectively.[31,32] With this choice, the simulation cell comprised a total of 36 chain molecules. Along the z axis, the "gliding-plane" boundary (GPB) conditions,[18] which combined a mirror plane at $z = L_z$ with a half-period translation along x, were used. That is, the space above the top face of the simulation cell was filled with a mirror image of the system shifted along x by $L_x/2$. (The shift is necessary to avoid highly correlated moves of a particle and its image across the mirror plane.) Because of the mirror plane at $z = L_z$, the substrate of the upper confining SAM occurs at $z = H = 2L_z$. The transformation of the x and z coordinates by the GPB conditions is

$$x' = x + kL_x/2 \quad (k = 1 \text{ for } x < L_x/2 \text{ and } k = -1 \text{ otherwise}) \quad (1)$$

$$z' = 2L_z - z \quad (2)$$

while the y coordinate remains unchanged. As a molecule leaves the simulation cell through the top face, its image, whose

coordinates are given by eqs 1 and 2, enters the cell through the other half of the top face.

Although the GPB conditions save nearly half the CPU time, they may, in principle, affect the simulation results because of the artificial correlations introduced by eqs 1 and 2 in the configuration of the system near the midplane $z = L_z = H/2$. To assess the importance of these correlations, a comparative simulation of two bulk water systems was made. One system was simulated using the usual periodic boundary conditions in all three dimensions. In the other system, the periodic boundary conditions were applied only along the *x* and *y* axes, while along the *z* axis, the system was replicated by applying the GPB conditions at $z = 0$ and $z = L_z$. The three lengths of the simulation box were set equal to 30 Å. The calculated quantities proved to be practically independent of whether the periodic or GPB conditions were used along the *z* axis.

A typical GCMC run comprised 5×10^6 passes, each composed of $N + N_s$ moves where N is the current number of water molecules and N_s is the number of chains in the SAM ($N_s = 36$). For the largest systems studied ($N \approx 800$), this corresponds to a total of 4×10^9 attempted configurations.

The hydration pressure was calculated from the equation[33]

$$p^h = \bar{f}/A - p^b \tag{3}$$

where p^b is the bulk water pressure, A is the surface area, $A = L_xL_y$, and $\bar{f}$ is the mean force exerted by the water molecules upon the lower SAM. In the separation range studied, the direct interaction between the SAMs did not exceed 3% of the solvent contribution to p^h, as given by eq 3, and so this interaction was neglected. The mean force in eq 3 is given by the equation

$$\bar{f} = \langle -\sum_I f_z^I \rangle = \left\langle \sum_{I,J} \sum_{i,j} \frac{\partial u(r^{I,i}, r^{J,j})}{\partial z_c^I} \right\rangle \tag{4}$$

where the angular brackets denote ensemble averaging, f_z^I is the *z* component of the force experienced by the *I*th water molecule because of its interactions with the confining SAMs, $u(r^{I,i}, r^{J,j})$ is the interaction energy between the *i*th force site on the *I*th water molecule and the *j*th atom in the *J*th chain molecule in the SAM; the differentiation is performed with respect to the *z* coordinate of the center of mass of the *I*th water molecule. With our choice of the *z* axis along the outward-pointing vector normal to the lower confining surface, positive values of p^h would correspond to attraction between the SAMs. To make our results consistent with the conventional choice of the sign of p^h,[34] we will hereafter refer to the values of p^h on the upper SAM so that positive p^h will correspond to repulsion, whereas negative p^h, to attraction.

Because of some penetration of water in the near-surface region of the SAMs, there was no clear-cut interface between the SAM and water, so the volume occupied by water remained uncertain. As a consequence, we could not calculate the average water density between the SAMs based on the ensemble average number of water molecules in the confined region, $\langle N \rangle$. As an alternative measure of the overall density depression or enhancement, the water density at the midpoint between the walls, $\rho_{H/2}$, was used. To smooth the statistical noise, the density distribution $\rho(z)$ near the midpoint was averaged over a certain interval Δ (typically, 3−5 Å) so that the exact definition for $\rho_{H/2}$ was

$$\rho_{H/2} = \Delta^{-1} \int_{H/2-\Delta}^{H/2} \mathrm{d}z\, \rho(z) \tag{5}$$

Clearly, the use of $\rho_{H/2}$ as a measure of density changes in the confined region made sense only when H was large enough for the water density oscillations near $H/2$ to decay.

In the calculations of the density profiles and other quantities dependent on the distance from the SAM substrate, the simulation box was divided into 100 slices of thickness $\Delta z = L_z/100$ lying parallel to the $x-y$ plane. During the GCMC run, the *z*-dependent quantities were averaged within each individual slice and then referred to the *z* coordinate of its center.

3. Results and Discussion

3.1. Bulk Water. Knowledge of the chemical potential of bulk water is a prerequisite of simulating confined water in the chemical equilibrium with the bulk water reservoir (see eq 3). For rigid water models such as TIP4P,[20] only the excess (nonideal) part of the chemical potential, μ', is required. An early MD simulation by Hermans et al.[35] using the thermodynamic integration method resulted, for the TIP4P model at room temperature, in a value of -5.3 kcal mol^{-1}, in satisfactory agreement with an experimental estimate of -5.7 kcal mol^{-1} based on the known ratio between the molar volumes of water vapor and liquid. Note that the Hermans et al. simulations[35] were made with a very small periodic system ($N = 80$) and a fairly short cutoff distance (6 Å). More recently, Shelley and Patey[21] reported a value of -6.0 kcal mol^{-1} as best reproducing the room-temperature bulk water density when the TIP4P model and Ewald summation method were employed.

To find μ' suited to the particular summation scheme, cutoff distance, and typical system size used in our simulations of confined water, we performed a series of bulk water simulations as a function of μ'. In these simulations, the periodic boundary conditions were used in all three dimensions. The experimental bulk water density at room temperature, $\rho^b = 0.997$ g cm^{-3}, was reproduced at $\mu' = -6.10$ kcal mol^{-1}, close to the Shelley and Patey result.[21] However, the respective bulk pressure, as calculated from the virial formula, proved to be 0.13 ± 0.03 kbar, which is somewhat higher than the atmospheric pressure. The desired pressure was obtained at $\mu' = -6.15$ kcal mol^{-1}. The corresponding equilibrium density was 0.991 g cm^{-3}, which is 0.6% lower than required. The observed small inconsistency between the calculated equilibrium pressure and density of TIP4P water is hardly surprising because the original fitting of the TIP4P model[20] to the experimental properties of water employed a different cutoff distance, number of molecules in the simulation cell, and statistical ensemble (*NPT*) than our simulations. In deciding between the two alternative values found for μ', our reasoning was that the "overpressure" of 0.13 kbar could be readily compensated for through eq 6, unlike the shift in density, which might have an unpredictable effect on the structural organization of water near confining surfaces. So the excess chemical potential of -6.10 kcal mol^{-1}, which exactly reproduced ρ^b and somewhat overestimated p^b, was adopted in all subsequent calculations.

3.2. Water Confined between Ag-Supported SAMs. It is known from ab initio electronic structure calculations[16,24] that the EG3-OMe tail favors a nearly helical conformation characterized by a trans−gauche−trans (tgt) configuration of the O−C−C−O bond sequences. A similar conformation is observed experimentally for the poly(ethylene glycol) (PEG) macromolecules in their crystals.[36] On the Ag substrate, the EG3-OMe-terminated alkanethiol molecules form an incommensurate crystal-like monolayer structure in which the EG3-OMe tails are in the all-trans planar conformation, as occur in stretched PEG crystals.[37] As shown by our static lattice energy

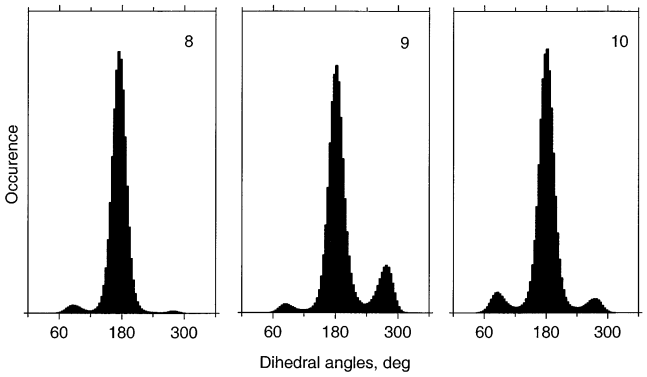

Figure 2. Distribution of the three terminal dihedral angles in the EG3-OMe tails for the Ag-supported SAM in contact with water. The angle numbers, *k*, correspond to the numbering system[20] in which the dihedrals are numbered in succession from 1 to 10 starting with the C−C−O−C dihedral angle at the junction of the alkanethiol chain and the EG3-OMe tail and ending at the C−C−O−Me dihedral in the terminal methoxy group.

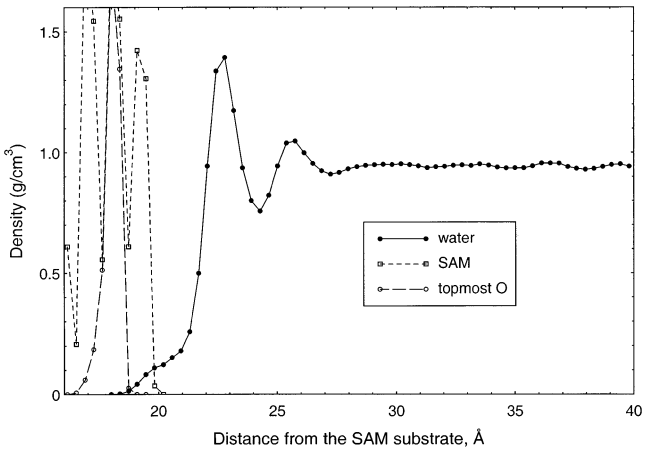

Figure 3. Density profiles of water, SAM, and topmost oxygen atoms of the methoxy groups near the interface formed by the Ag-supported SAM and water.

calculations,[26] the driving force behind the transition from the helical to all-trans conformation in the EG3-OMe-terminated SAM is a substantial increase in the packing density, which forces the EG3-OMe tails to assume a more extended conformation favorable for packing.

The simulation results for the distribution of dihedral angles in the EG3-OMe tails when in contact with water show a noticeable concentration of gauche defects close to the chain ends (Figure 2). The appearance of these defects is partly associated with the formation of hydrogen bonds between the topmost oxygen atoms of the EG3-OMe tails and the water molecules. In the density profiles shown in Figure 3, the water molecules involved in the hydrogen bonding with the SAM are seen as a shoulder on the low-density edge of the water density distribution $\rho(z)$. The overlap of the shoulder with the profile of the SAM density is indicative of some penetration of water into the SAM down to the topmost oxygen atoms. Note that the ability of individual water molecules to form hydrogen bonds with the topmost oxygen atoms of the Ag-supported SAM could not be detected in the ab initio static energy calculations by Wang et al.[16] owing to the neglect of thermal motion of both the water and EG3-OMe molecules.

Evaluation of the average number of hydrogen bonds formed by water molecules with the SAM during the GCMC run shows, however, that only 17% of the EG3-OMe-terminated alkanethiol chains are hydrogen bonded to water. About 35% of these hydrogen bonds enter into bridged intermolecular bonds in which one water molecule is bound to two different chains in the SAM. On the basis of the areal density of the SAM and the percentage of the chains involved in hydrogen bonding with water, it is easy to calculate that the areal density of the surface sites supplied by the SAM for hydrogen bonding with water is as low as 0.01 Å^{-2}, about 7 times less than a lattice-model estimate of the value needed to match that of bulk water.[9] That is, despite the ability of the SAM to form hydrogen bonds with water, there is no reason to expect that the SAM will show hydrophilic behavior.

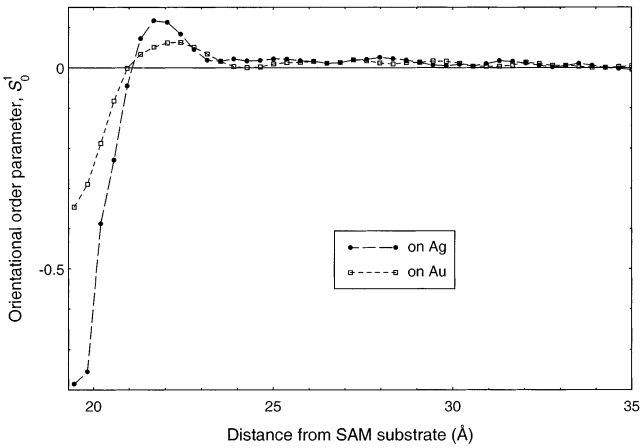

Figure 4. Orientational order parameter S_0^1 in water layers adjacent to the Ag- and Au-supported SAMs.

The amphiphilic nature of the SAM surface manifests itself in the orientational distribution of water molecules in the interface region. This can be appreciated from Figure 4, which presents the distance dependence of the orientational order parameter, $S_0^1 = \langle \cos \theta \rangle$, where θ is the angle formed by the molecular dipole moment with the z axis. The orientational ordering induced by the SAM is short-ranged and affects only the molecules in the first hydration layer ($z < 24$ Å). For the majority of these molecules, corresponding to the main peak of the density distribution, the dipole moments point preferentially outward from the SAM ($S_0^1 > 0$), which is typical of hydrophobic surfaces.[38] By contrast, the few water molecules that are directly involved in hydrogen bonding with the EG3-OMe chains have their dipole moments pointing inward toward the SAM, as it occurs near hydrophilic proton-acceptor surfaces.[39]

The effect of the SAM on the lateral distribution of water molecules in the adjacent water layers is fairly small. As an example, Figure 5 compares the pair distribution function in the slice centered at the main density maximum with that in water bulk. The differences are a somewhat more pronounced first density peak and a slight shift of the density oscillations to a longer wavelength.

Because of the dominance of hydrophobic areas on the SAM surface, the approach of a water molecule to the SAM is, on the average, energetically unfavorable. This can be seen from Figure 6, which shows the distance dependence of the average interaction energy of a water molecule with its surroundings, $\psi(z)$ (i.e., the enthalpic part of the local chemical potential of water). At separations near the first density maximum, ψ loses about 2 kcal/mol in magnitude compared to that in water bulk (Figure 6). As the molecule comes closer to the SAM surface, the energy loss is first partly compensated by the formation of

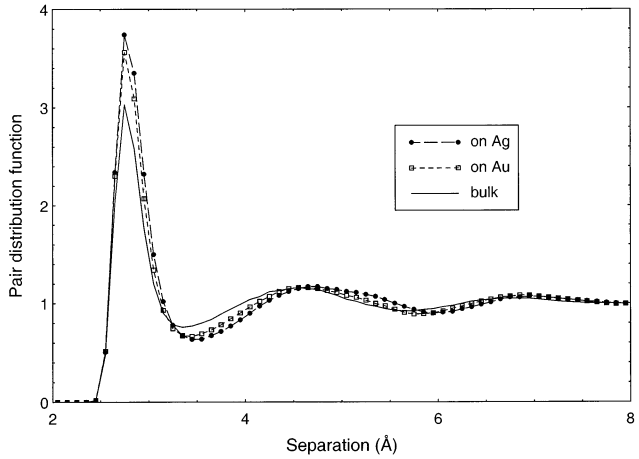

Figure 5. Pair distribution functions of water in slices corresponding to the main maximum of the water density profile for the Ag- and Au-supported SAMs in comparison with that for bulk water.

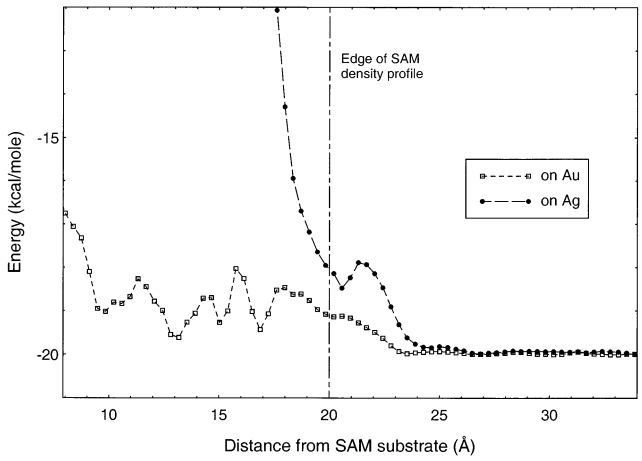

Figure 6. Average interaction energy of a water molecule with its surroundings in the SAM−water interface region for the Ag- and Au-supported SAMs.

TABLE 1: Midpoint Density and Hydration Pressure for Water Confined between EG3-OMe-Terminated Alkanethiol SAMs

H (Å)	H_0 (Å)	$\rho_{H/2}$ (g/cm^3)[a]	p^h (kbar)[a]
		on Ag substrate	
≤72	≤32	cavitation	
76	36	0.938	−0.51
80	40	0.944	−0.39
100	60	0.974	not converged
		on Au substrate	
≤58	≤18	cavitation	
60	20	*b*	−0.80
72	32	0.945	−0.43
80	40	0.951	−0.31
100	60	0.964	−0.04

[a] At $H \leq 80$ Å, the statistical uncertainty in $\rho_{H/2}$ and p^h was estimated to be 0.004 g/cm^3 and 0.05 kbar, respectively. At $H = 100$ Å, the uncertainty in p^h was at least 0.1 kbar for the Au-supported SAM, whereas for the Ag-supported SAM, p^h was not converged at all. [b] $\rho_{H/2}$ was not evaluated because of perceptible density oscillations near $H/2$.

hydrogen bonds with the SAM, and then the magnitude of ψ rapidly drops mainly because of the loss of water−water interactions.

We now turn to our results for the hydration pressure p^h and midpoint density $\rho_{H/2}$, which are summarized in Table 1. In our simulations, we have tried some selected separations H covering the range 60 Å $\leq H \leq$ 100 Å. The SAM thickness, h, as determined from the low-density edge of the SAM density distribution (Figure 3), was about 20 Å and was practically independent of H. So the thickness of the slit between the SAM surfaces, $H_0 = H - 2h$, ranged from 20 to 60 Å. At all attempted $H_0 \leq 32$ Å, the system experienced capillary evaporation (cavitation) typical of water confined between hydrophobic surfaces: starting with a certain length of the GCMC run, the number of water molecules sharply decreased until nearly all of the molecules left the confined region. At higher separations, the system showed attractive p^h and noticeably depressed $\rho_{H/2}$, which is also characteristic of hydrophobic surfaces.[34] It is important that the calculated magnitude of p^h substantially exceeds the upper limiting value of p^h because of the pressure imbalance caused by cavitation, $p^h \leq p^b$ (0.13 kbar in our case). Similar results were obtained in simulations of water between structureless hydrophobic surfaces.[39] All this means that the interpretation of the hydrophobic attraction solely in terms of cavitation or "drying"[8] can hardly provide a comprehensive description of this phenomenon.

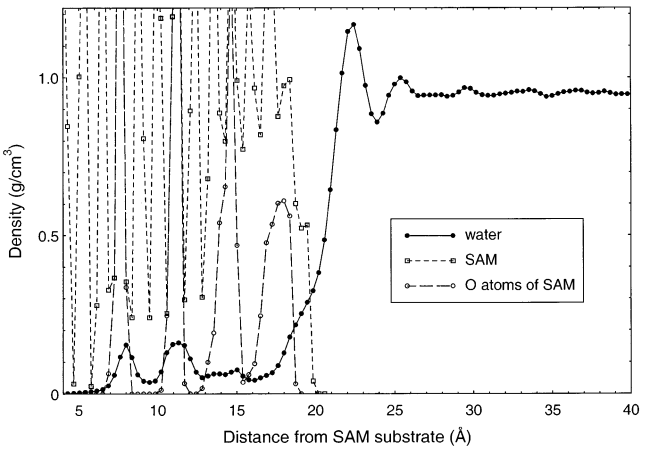

Figure 7. Density profiles of water, SAM, and oxygen atoms of the EG3-OMe tails near the interface formed by the Au-supported SAM and water.

3.3. Water Confined between Au-Supported SAMs. In a dry atmosphere, the EG3-OMe-terminated alkanethiol SAMs prepared on the Au substrate form a structure in which the EG3-OMe tails assume a helixlike conformation similar to that observed in isolated OEG molecules and PEG crystals.[15,16,24,36] The lattice of the sulfur headgroups in the Au-supported SAMs is dictated by the headgroup−substrate interactions and is commensurate with the Au(111) lattice. The alkane chains are tilted by ∼35° with respect to the surface normal.[32] The separation between the sulfur headgroups in the SAM is about 5 Å, which is substantially greater than the equilibrium separation between the alkane chains (∼4.6 Å).

According to the SFG measurements by Zolk et al.,[17] the contact with water causes a substantial conformational disordering and penetration of water into the SAM. This experimental finding is well supported by our computer simulations. The penetration of water molecules deep into the EG3-OMe layer of the SAM can be appreciated from the water and SAM density profiles in Figure 7. Note that the water density distribution within the SAM shows maxima that correlate with the positions of the ether oxygen atoms, thus demonstrating the tendency of the water molecules to form hydrogen bonds with the EG3-OMe chains. The conformational disordering caused by the water molecules in the SAM can be seen well in the distribution of the dihedral angles in the EG3-OMe tails (Figure 8). An important result is that the EG3-OMe tails assume, on the average, more-extended conformations compared to that ob-

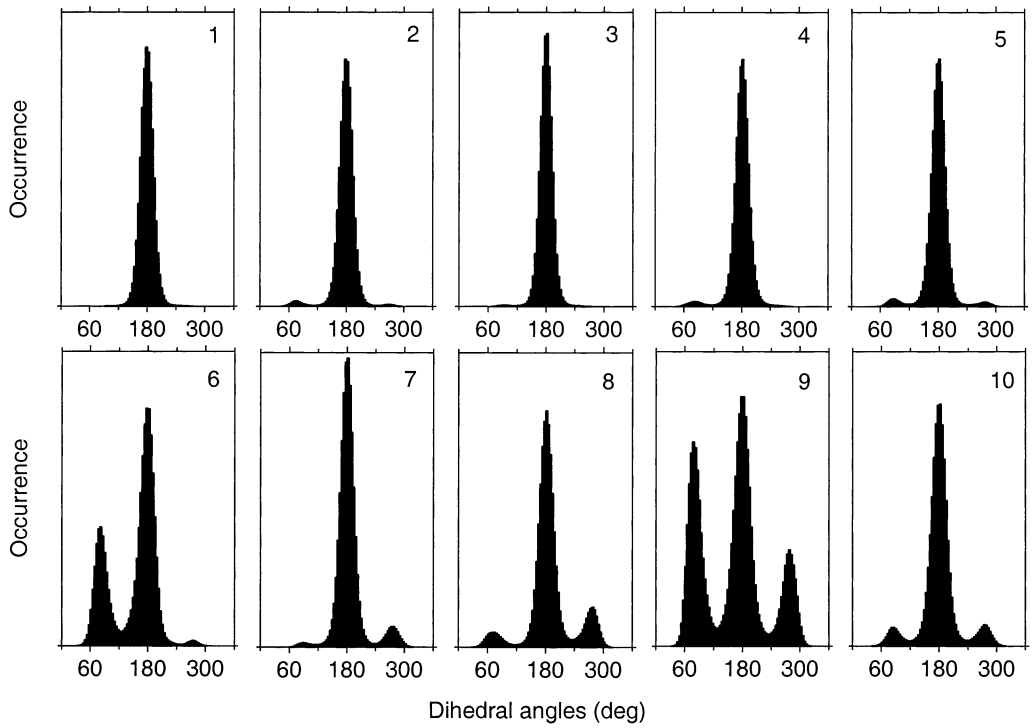

Figure 8. Distribution of dihedral angles in the EG3-OMe tails for the Au-supported SAM in contact with water (see caption to Figure 2 for atom numbering).

served in the dry SAM. In these conformations, most of the former gauche conformers around the C−C bonds give way to trans conformers (see dihedrals 3, 6, and 9 in Figure 8) so that the most-populated conformer of the EG3-OMe tails becomes all trans. The tails are in a nearly upright orientation similar to that observed in the SAM on Ag. The net result of these changes is that the contact with water makes the SAM thickness practically independent of the substrate used (∼20 Å, see Figures 3 and 7). Since the areal densities of the sulfur headgroups in the Au- and Ag-supported SAMs are related as $(4.6/5.01)^2 \approx 0.84$, the volume density of the former proves to be 16% lower than that of the latter. It is this difference in density that provides the space for the accommodation of water molecules within the Au-supported SAM.

To make sure that the above-described structure of the SAM−water interphase region is representative of the equilibrium state of the system, three independent GCMC runs starting from different configurations were carried out. One starting configuration was taken to be the final configuration obtained in our previous studies.[18] The other two configurations were constructed by attaching a slab of bulk water, as simulated using the periodic boundary conditions in all three dimensions, to two different configurations of the SAM, one built up from ideal tgt helices and the other from ideal all-trans zigzags. After $\sim 10^7$ GCMC passes, all three runs converged to nearly the same structure, as characterized by the distributions of density and dihedral angles.

The loss of stability of the helical tgt conformer on going from the dry Au-supported SAM to that in contact with water can be explained in the following way. As shown by the ab initio SCF calculations by Wang et al.,[16] a perfect close packing of the helical chains on a hexagonal lattice with a period of 5 Å does not allow water molecules to penetrate into the SAM to form hydrogen bonds with the next-to-the-topmost and deeper oxygen atoms. These oxygen atoms can be reached by water molecules only if the EG3-OMe chains assume more-extended conformations and a nearly upright orientation relative to the substrate surface. That is, the loss in the conformational energy of the EG3-OMe chains is compensated for by the formation of hydrogen bonds between the penetrated water molecules and the three inner oxygen atoms of the chains. By integrating the water density distribution in Figure 7 within the SAM−water interpenetration range (from 5 to 20 Å), we obtain 36 penetrated water molecules per simulation cell (i.e., one water molecule per EG3-OMe chain). All of these molecules are involved in hydrogen bonds with the ether oxygen atoms; 44% of the water molecules are bound to the topmost oxygen atoms, and the remaining 56%, to the three deeper oxygens. About 20% of the hydrogen bonds formed by water with the EG3-OMe chains are bridged bonds, and all of these latter bonds are intermolecular.

Compared to the situation near the Ag-supported SAM, the approach of a water molecule to the surface of the SAM prepared on Au is associated with a noticeably smaller loss in the magnitude of ψ (∼0.5 kcal/mol for molecules in the vicinity of the first density maximum, see Figure 6). Because of the conformational disordering of the EG3-OMe chains and the diffuse character of the SAM−water interface, the orienting effect of the SAM on the adjacent water layers is insignificant (Figure 4). The effect of the SAM on the lateral distribution of water molecules is also insignificant—less than that observed near the Ag-supported SAM (Figure 5). Thus, a remarkable feature of the EG3-OMe-terminated SAM on Au is that it perturbs the structure and energetics of the contiguous water layers only slightly.

At all attempted separations in the interval 60 Å $\leq H \leq$ 100 Å, corresponding to slit widths H_0 between 20 and 60 Å, the hydration pressure p^h is attractive, and $\rho_{H/2}$, depressed (Table 1). In addition, at $H \leq 58$ Å ($H_0 \leq 18$ Å), water confined between the Au-supported SAMs shows capillary evaporation. That is, similar to the SAM on Ag, the Au-supported SAM behaves like a hydrophobic surface. It should, however, be noted that the capillary evaporation between the Au-supported SAMs occurs at a substantially smaller slit width compared to that

between the Ag-supported SAMs (18 vs 32 Å). In this respect, the former can be regarded as being less hydrophobic.

The simulation results for the hydration forces operating between the EG3-OMe-terminated SAMs can be compared with the recent surface-force measurements by Dicke et al.[14] using scanning force microscopy. The experiments were performed in aqueous solutions of KNO_3 in a concentration range from 0.1 mM to 0.1 M. The Ag-supported SAMs exhibited a hydrophobic attraction that was practically independent of the ion concentration. The behavior of the Au-supported SAMs was more complicated. At low ion concentrations, the SAMs showed a long-range repulsion that rapidly weakened with increasing ion concentration. At the highest ion concentration used (0.1 M), the repulsion of the EG3-OMe-terminated SAMs changed to attraction.

Whereas the experimental results[14] for the Ag-supported SAM are in agreement with our GCMC simulations, the data for the Au-supported SAM are not. Since the simulations reproduce only the force that corresponds to ideally pure and nondissociable water, the discrepancy between the simulation and the experiment can well be attributed to the ions present in water. The same conclusion can be drawn from the experimentally observed strong dependence of the surface force on the electrolyte concentration.[14] Direct evidence for the occurrence of an electric charge at the interface formed by the SAM and aqueous electrolyte solutions has recently been obtained by Chan et al.[40] using electrokinetic measurements. The charge was found to be positive at pH $<$ 4.4 and negative otherwise. That is, even in neutral water the interface bore a negative charge.

The origin of the SAM−water interfacial charge has not yet been conclusively established. The recent surface-force measurements by Dicke and Hähner[41] show, however, that the surface force is only slightly dependent on the electrolyte used and is governed mainly by pH. That is, the interfacial negative charge originates most likely from an asymmetric adsorption of the products of water autodissociation, viz., from the preferential adsorption of hydroxide, OH^-, over hydronium, H_3O^+, as occurs in thin aqueous foam films stabilized by OEG *n*-alkyl surfactants.[42] The difference in the surface-force behavior between the Ag- and Au-supported SAMs can then be explained in terms of the difference in their packing densities. In the case of the Ag-supported SAM, its high packing density prevents the ions from incorporation into the SAM. As a consequence, the near-surface region of the SAM remains electrically neutral, and the interaction force is dominated by the hydrophobic attraction, as predicted by our simulations. By contrast, the structural changes occurring in the Au-supported SAM in contact with water may allow the penetration and subsequent capture of the OH^- and H_3O^+ ions in the EG3-OMe layer of the SAM. Since OH^- forms less-stable hydration structures,[43] it may escape more easily from its hydration shell and penetrate into the EG3-OMe layer in larger amounts. The resulting charge separation should lead to the electrostatic repulsion of the opposite SAM surfaces, as described by the DLVO theory.[3] At high electrolyte concentrations, the surface charge is screened by counterions in solution, with the result that the hydrophobic attraction becomes dominant.

4. Conclusions

In this work, we have simulated the hydration forces operating between the EG3-OMe-terminated SAMs on the Au and Ag substrates. As far as we know, this is the first simulation study of the water-mediated forces between organic surfaces that is based on a realistic molecular model and force field. Despite the experimentally observed water wetability of the SAMs (the water contact angle being ∼60° for both SAMs on Au and Ag substrates[15]), the effect of the SAMs on confined water is typical of hydrophobic surfaces. The main manifestations of hydrophobicity are first the capillary evaporation experienced by water at small separations and second an attractive hydration pressure in conjunction with a noticeably reduced water density level between the SAMs.

The simulations described in this paper suggest that the fundamental difference between the Ag- and Au-supported SAMs is the lower areal density of the latter. Because of this difference, the Au-supported SAM is penetrable to water, whereas the SAM prepared on Ag is not. The penetration of water deep into the Au-supported SAM is accompanied by conformational disordering and a redistribution of conformer populations such that the helical conformation practically disappears and the most-populated conformer of the EG3-OMe tails becomes all trans. It is likely that the looser structure of the Au-supported SAM also makes it selectively penetrable to the OH^- ions, which may explain the difference in the behavior of the Au- and Ag-supported SAMs in surface-force experiments.[15]

The simulations show that the effect of the Au-supported SAMs on the structure of the adjacent water layers is remarkably small. In view of this finding, the protein resistance of the SAM can hardly be ascribed to a protective coat of structured water, as is frequently speculated in the chemical and biological literature to explain the force preventing colloid particles, macromolecules, or surfaces from having direct contact.[3] The hydration force cannot explain the protein resistance; both the Au- and Ag-supported SAMs behave as a hydrophobic surface and so should both attract the hydrophobic parts of the protein molecule. The relevance of the negative surface charge acquired by the Au-supported SAM[40] to its protein resistance is vague because a similar negative charge is observed on the surface of unsubstituted C16 and C18 alkanethiol SAMs,[44] which are not protein resistant. Thus, the origin of the protein resistance of the EG3-OMe-terminated SAM on Au, as opposed to that on Ag, still remains to be understood. The only simulation result, which conforms with the observed difference in the protein adsorption behavior of the SAMs, is the markedly higher areal density of hydrogen bonds formed by water with the topmost oxygen atoms of the Au-supported SAM (∼0.03 $Å^{-2}$) compared to that on Ag (0.01 $Å^{-2}$). Since the adsorption of a protein molecule on the SAM surface involves the dehydration of (at least) the topmost oxygen atoms, this factor should indeed make the Au-supported SAM more resistant to protein adsorption. Of some relevance to the protein resistance of the Au-supported SAM may also be the microscopic roughness or "diffusivity" of its interface with water, which results from the conformational disordering of the EG3-OMe chains. This diffusivity should reduce the contact area of the protein molecule with the SAM, thereby reducing the probability of adsorption.

Acknowledgment. This paper is dedicated to Professor Walter Siebert on his 65th birthday. This work was supported by the Deutsche Forschungs-Gemeinschaft, the Office for Naval Research, and the Fond der Chemischen Industrie.

References and Notes

(1) Israelachvili, J.; Wennerström, H. *Nature (London)* **1996**, *379*, 219.
(2) Vogler, E. A. *Adv. Colloid Interface Sci.* **1998**, *74*, 69.
(3) Israelachvili, J. *Intermolecular and Surface Forces*; Academic Press: London, 1992. Lyklema, J. *Fundamentals of Interface and Colloid Science*; Academic Press: London, 1991.

(4) Rand, R. P.; Parsegian, V. A. *Biochim. Biophys. Acta* **1989**, *778*, 224. Parsegian, V. A. *Adv. Colloid Interface Sci.* **1982**, *16*, 49.
(5) Podgornik, R. *J. Chem. Phys.* **1989**, *91*, 5840.
(6) Ash, S. G.; Everett, D. H.; Radke, C. *J. Chem. Soc., Faraday Trans. 2* **1973**, *84*, 1256.
(7) Ruckenstein, E.; Churaev, N. *J. Colloid Interface Sci.* **1991**, *147*, 535. Tsao, Y.; Evans, D. F.; Wennerström, H. *Science (Washington, D.C.)* **1993**, *262*, 547. Parker, J. L.; Claesson, P. M.; Attard, P. *J. Phys. Chem.* **1994**, *98*, 8468.
(8) Lum, K.; Chandler, D.; Weeks, J. D. *J. Phys. Chem. B* **1999**, *103*, 4570.
(9) Besseling, N. A. M. *Langmuir* **1997**, *13*, 2113.
(10) Ulman, A. *An Introduction to Ultrathin Organic Films*; Academic Press: Boston, 1991. Ulman, A. *Chem. Rev.* **1996**, *96*, 1533.
(11) Schreiber, F. *Prog. Surf. Sci.* **2000**, *65*, 151.
(12) Hautman, J.; Klein, M. L. *J. Chem. Phys.* **1989**, *91*, 4994. Hautman, J.; Klein, M. L. *J. Chem. Phys.* **1990**, *93*, 7483. Hautman, J.; Bareman, J. P.; Mar, W.; Klein, M. L. *J. Chem. Soc., Faraday Trans.* **1991**, *87*, 2031. Mar, W.; Klein, M. L. *Langmuir* **1994**, *10*, 188. Siepmann, J. I.; McDonald, I. R. *Mol. Phys.* **1992**, *2*, 255. Siepmann, J. I.; McDonald, I. R. *Langmuir* **1993**, *9*, 2351.
(13) Prime, K. L.; Whitesides, G. M. *J. Am. Chem. Soc.* **1993**, *115*, 10714.
(14) Dicke, C.; Feldman, K.; Eck, W.; Herrwerth, S.; Hähner, G. *Polym. Prepr. (Am. Chem. Soc., Div. Polym. Chem.)* **2000**, *41*, 1444.
(15) Harder, P.; Grunze, M.; Dahint, R.; Whitesides, G. M.; Laibinis, P. E. *J. Phys. Chem. B* **1998**, *102*, 426.
(16) Wang, R. L. C.; Kreuzer, H. J.; Grunze, M. *J. Phys. Chem.* **1997**, *101*, 9767.
(17) Zolk, M.; Eisert, F.; Pipper, J.; Herrwerth, S.; Eck, W.; Buck, M.; Grunze, M. *Langmuir* **2000**, *16*, 5849.
(18) Pertsin, A. J.; Grunze, M. *Langmuir* **2000**, *16*, 8829.
(19) Compared to our previous work,[16] the present simulations refer to a somewhat different value of the chemical potential. In addition, a more efficient sampling procedure is used, which allows us to bring the system closer to the equilibrium state. For these reasons, the results of the present simulations show some differences from those reported in the earlier work.[16]
(20) Jorgensen, W. L.; Chandrasekhar, J.; Madura, J. D.; Impey, R. W.; Klein, M. L. *J. Chem. Phys.* **1983**, *79*, 926.
(21) Shelley, J. C.; Patey, G. N. *Mol. Phys.* **1996**, *88*, 385.
(22) Smith, G. D.; Jaffe, R. L.; Yoon, D. Y. *J. Phys. Chem.* **1993**, *97*, 12752. Bedrov, D.; Pekny, M.; Smith, G. D. *J. Phys. Chem. B* **1998**, *102*, 996.
(23) Pertsin, A. J.; Hayashi, T.; Grunze, M. *Phys. Chem. Chem. Phys.* **2001**, *3*, 1598.
(24) Wang, R. L. C.; Kreuzer, H. J.; Grunze, M. *Phys. Chem. Chem. Phys.* **2000**, *2*, 3613.
(25) Sorensen, R. A.; Liau, W. B.; Kesner, L.; Boyd, R. H. *Macromolecules* **1988**, *21*, 200.
(26) Pertsin, A. J.; Grunze, M. *Langmuir* **1994**, *10*, 3668.
(27) Allen, M. P.; Tildesley, D. J. *Computer Simulation of Liquids*; Clarendon Press: Oxford, U.K., 1993.
(28) Stapleton, M. R.; Panagiotopoulos, A. *J. Chem. Phys.* **1990**, *92*, 1285.
(29) Swendsen, R. H.; Wang, J.-S. *Phys. Rev. Lett.* **1987**, *58*, 86.
(30) Pertsin, A. J.; Hahn, J.; Grossmann, H.-P. *J. Comput. Chem.* **1994**, *15*, 1121.
(31) Fenter, P.; Eisenberger, P.; Li, J.; Camilone, N., III; Bernasek, S.; Scoles, G.; Ramanarayanan, T. A.; Liang, K. S. *Langmuir* **1991**, *7*, 2013. Samant, M. G.; Brown, C. A.; Gordon, J. G., II. *Langmuir* **1993**, *9*, 1082. Camilone, N.; Chidsey, C. E. D.; Liu, G.-Y.; Scoles, G. *J. Chem. Phys.* **1993**, *98*, 3503.
(32) Pertsin, A. J.; Grunze, M.; Garbuzova, I. A. *J. Phys. Chem. B* **1998**, *102*, 4843.
(33) Evans, R.; Marconi, U. M. B. *J. Chem. Phys.* **1987**, *86*, 7138.
(34) Forsman, J.; Jönsson, B.; Woodward, C. E. *J. Phys. Chem.* **1996**, *100*, 15005.
(35) Hermans, J.; Pathiaseril, A.; Anderson, A. *J. Am. Chem. Soc.* **1988**, *110*, 5982.
(36) Takahashi, Y.; Tadokoro, H. *Macromolecules* **1973**, *6*, 672.
(37) Takahashi, Y.; Sumita, I.; Tadokoro, H. *J. Polym. Sci.* **1973**, *11*, 2113.
(38) Lee, S. H.; Rossky, P. J. *J. Chem. Phys.* **1994**, *100*, 3334.
(39) Hayashi, T.; Pertsin, A. J.; Grunze, M. *J. Chem. Phys.* **2002**, *117*, 6271.
(40) Chan, M.; Schweiss, R.; Werner, C.; Grunze, M. To be submitted for publication.
(41) Dicke, C.; Hähner, G. *J. Phys. Chem. B* **2002**, *106*, 4450. Dicke, C.; Hähner, G. Private communication.
(42) Karraker, K. A.; Radke, C. J. *Adv. Colloid Interface Sci.* **2002**, *96*, 231.
(43) Friedman, H. L.; Krishnan, C. V. Thermodynamics of Ion Hydration. In *Water: A Comprehensive Treatise;* Frank, F., Ed.; Plenum Press: London, 1973; Vol. 3, p. 72.
(44) Schweiss, R.; Welzel, P. B.; Werner, C.; Knoll, W. *Langmuir* **2001**, *17*, 4304.